01 Jun 2016

Shear Wave Splitting Analyses in Tian Shan: Geodynamic Implications of Complex Seismic Anisotropy

Solomon G. Cherie

Stephen S. Gao
Missouri University of Science and Technology, sgao@mst.edu

Kelly H. Liu
Missouri University of Science and Technology, liukh@mst.edu

Ahmed A. Elsheikh

et. al. For a complete list of authors, see https://scholarsmine.mst.edu/geosci_geo_peteng_facwork/412

Recommended Citation

S. G. Cherie et al., "Shear Wave Splitting Analyses in Tian Shan: Geodynamic Implications of Complex Seismic Anisotropy," *Geochemistry, Geophysics, Geosystems*, vol. 17, no. 6, pp. 1975-1989, John Wiley & Sons Ltd, Jun 2016.
The definitive version is available at https://doi.org/10.1002/2016GC006269

AGU PUBLICATIONS

Geochemistry, Geophysics, Geosystems

RESEARCH ARTICLE
10.1002/2016GC006269

Shear wave splitting analyses in Tian Shan: Geodynamic implications of complex seismic anisotropy

Solomon G. Cherie[1], Stephen S. Gao[1], Kelly H. Liu[1], Ahmed A. Elsheikh[1], Fansheng Kong[1], Cory A. Reed[1], and Bin B. Yang[1]

[1]Geology and Geophysics Program, Missouri University of Science and Technology, Rolla, Missouri, USA

Key Points:
- Systematic azimuthal variations of splitting parameters are found at 15 of 25 sites in Tian Shan
- Modeling shows the upper layer of anisotropy is from N-S lithospheric shortening
- Anisotropy in the lower layer is caused by mantle flow driven by Tarim subduction

Correspondence to:
S. S. Gao,
sgao@mst.edu

Citation:
Cherie, S. G., S. S. Gao, K. H. Liu, A. A. Elsheikh, F. Kong, C. A. Reed, and B. B. Yang (2016), Shear wave splitting analyses in Tian Shan: Geodynamic implications of complex seismic anisotropy, *Geochem. Geophys. Geosyst.*, *17*, 1975–1989, doi:10.1002/2016GC006269.

Received 22 JAN 2016
Accepted 5 MAY 2016
Accepted article online 10 MAY 2016
Published online 9 JUN 2016

Abstract The Tian Shan is a tectonically complex intracontinental orogenic belt situated between the Tarim Basin and the Kazakh Shield. The vast majority of the previous shear wave splitting (SWS) measurements were presented as station averages, which are only valid when the anisotropy structure can be approximated by a single layer of anisotropy with a horizontal axis of symmetry, i.e., a model of simple anisotropy. A variety of anisotropy-forming hypotheses have been proposed based on the station-averaged measurements. In this study, we measure the splitting parameters at 25 stations that recorded high-quality data from a wide back azimuthal range for the purpose of identifying and characterizing complex anisotropy. Among the 25 stations, 15 of them show systematic azimuthal variations in the observed splitting parameters with a 90° periodicity that is consistent with a model of two-layered anisotropy. The fast orientations of the upper layer range from 50° to 90° measured clockwise from the north, which are subparallel to the strike of the orogenic belt, and the splitting times are between 0.9 and 1.9 s. The corresponding values for the lower layer are −45° to −85° and 1.2–2.2 s, respectively. The remaining 10 stations demonstrate azimuthally invariant splitting parameters with strike-parallel fast orientations, and can be represented by a single layer of anisotropy with a horizontal axis of symmetry. We propose that the strike-parallel anisotropy is caused by lithospheric shortening, and anisotropy in the lower layer is associated with WNW-ward flow of asthenospheric material sandwiched between the subducting Tarim lithosphere and the thick Kazakh lithospheric root.

1. Introduction

The Tian Shan Orogenic Belt (TSOB; Figure 1), situated between the Tarim Basin to the south and the Kazakh Shield to the north, resides within the extensive tectonic influence of the India-Eurasia collisional field [e.g., *Allegre et al.*, 1984; *Yin*, 2010]. Closure of the Paleo-Asian Ocean during the late Paleozoic to Early Mesozoic and associated accretion of island arcs and collision contributed to the buildup of the Tian Shan range, which is a well-developed intracontinental orogenic belt constituting the southwestern margin of the Central Asian Orogenic Belt [*Sengor et al.*, 1993; *Glorie et al.*, 2011]. Far-field stresses emanating from the collision of the Indian and Eurasian plates during the Cenozoic later induced a reactivation of the TSOB [*Avouac et al.*, 1993]. The surface topography and tectonic structures such as thrust and strike-slip faults observed in the TSOB are surficial expressions of lithospheric deformation resulting from the Cenozoic collision [*Thompson et al.*, 2002; *Vinnik et al.*, 2006; *Li et al.*, 2010]. Various strike-parallel mountain ranges and inter-range basins comprise a belt of extensive deformation characterized by significant seismicity [*Guo et al.*, 2006] with reported magnitudes exceeding values of 8 [*Zubovich et al.*, 2010]. A major dextral strike-slip fault, the Talasso-Fergana fault (Figure 1), separates the western and central TSOB [*Makeyeva et al.*, 1992]. Based on GPS measurements and earthquake focal mechanism studies, the TSOB is believed to undergo significant N-S crustal shortening at a rate of ~20 mm/yr [*Abdrakhmatov et al.*, 1996] whereas the Tarim Basin is relatively resistant to significant deformation [*Neil and Houseman*, 1997] and acts as a rigid body to transfer compressional stresses to the Tian Shan region.

The upper mantle structure beneath the TSOB and adjacent areas has been investigated by a number of seismic tomography studies. *Guo et al.* [2006] carried out seismic tomography analyses using P-arrivals recorded by portable seismic arrays across the Chinese Tian Shan and regional seismic networks. They imaged the velocity structure of the crust and upper mantle down to 400 km depth. The resulting crustal structure suggests that the Tian Shan crust is strongly squeezed by the Tarim Block. Additionally, the authors suggested the existence of low-velocity anomalies at

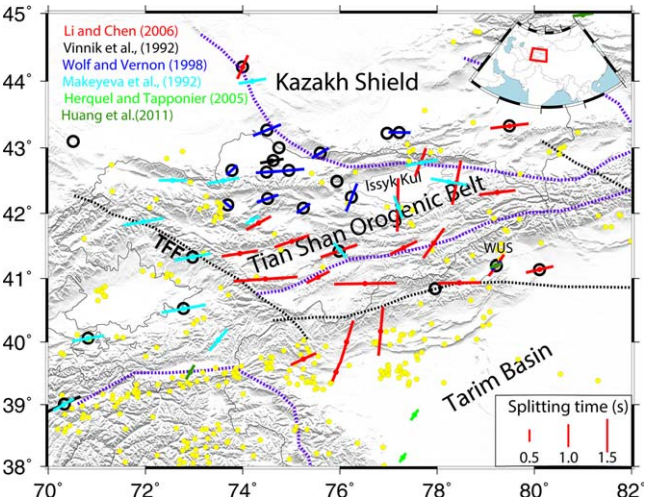

Figure 1. Topographic base map showing previous SWS measurements in the Tian Shan and adjacent areas. The orientation of the bar represents the fast polarization direction and the length of the bar is proportional to the splitting time. Open circles represent stations used in this study. Blue dotted lines represent major tectonic boundaries, black dashed lines are major faults, and yellow circles are magnitude 5.0 or greater earthquakes occurred between 1 January 1980 and 31 March 2015. TFF: Talasso-Fergana fault.

a depth of 150–400 km beneath the Tarim and Junggar Blocks. A teleseismic tomographic study by *Lei and Zhao* [2007] using 7176 high-quality *P* wave arrivals revealed a high-velocity block with a 60 km diameter extending down to the mantle transition zone. Based on this finding, the authors suggested a southward and northward underthrusting of the Kazakh Shield and Tarim Basin, respectively, beneath the Tian Shan.

Investigating lithospheric and mantle dynamics using the shear wave splitting (SWS) technique is a fundamental step toward understanding the kinematics of orogenesis as well as the relationship between mantle deformation and seismic anisotropy [*Silver and Chan*, 1991; *Makeyeva et al*., 1992; *Wolfe and Vernon*, 1998; *Savage*, 1999; *Becker et al*., 2003; *Long and Silver*, 2009; *Liu et al*., 2014]. Mantle deformation produces lattice preferred orientation (LPO) of mantle anisotropic minerals, primarily olivine, from which we are able to examine the polarization orientation and the magnitude of strain [*Nicolas and Christensen*, 1987; *Zhang and Karato*, 1995]. Specifically, simple shear associated with a mantle flow field tends to align the olivine *a* axis along the flow direction in areas dominated by A-type olivine fabrics, which is the most abundant among the five fabric types [*Ben Ismail and Mainprice*, 1998; *Long and Silver*, 2009; *Ohuchi and Irifune*, 2013]. Thus, splitting of P-to-S converted phases on the receiver side of the core-mantle boundary, including the PKS, SKKS, and SKS (which are hereafter referred to as XKS) phases, is utilized to understand lithospheric and asthenospheric LPO [*Silver*, 1996; *Savage*, 1999; *Fouch and Rondenay*, 2006; *Gao and Liu*, 2009; *Long and Silver*, 2009; *Gao et al*., 2010].

When seismic shear waves travel through anisotropic media, they split into orthogonal fast and slow waves; the resulting pair of splitting parameters is defined by ϕ, the polarization orientation of the fast wave, and δt, the delay time between the fast and slow components [*Silver and Chan*, 1991; *Vinnik et al*., 2007; *Liu et al*., 2008; *Long and Silver*, 2009]. The polarization orientation of the fast wave is often interpreted as either parallel to mantle flow, parallel to the strike of subvertical lithospheric dikes, or normal to the maximum compressional stress [*Karato*, 1989; *Silver and Chan*, 1991; *Gao et al*., 1994, 1997; *McNamara et al*., 1994; *Bokelmann et al*., 2013].

Under the simple anisotropy model which refers to a single layer of azimuthal anisotropy with a horizontal axis of symmetry, the splitting parameters are invariant with respect to the back azimuth (BAZ) of the XKS event. On the other hand, for most forms of complex anisotropy models, the parameters measured under the assumption of simple anisotropy are systematic functions of the BAZ [*Silver and Savage*, 1994], and therefore, the observed splitting parameters are apparent rather than true parameters for complex anisotropy. The apparent splitting parameters for the simplest form of complex anisotropy, which is composed of two layers of simple anisotropy with nonparallel and nonorthogonal fast orientations ("two-layered anisotropy"), have a 90° periodicity with respect to the BAZ, i.e., $P(\theta)=P(\theta+90n)$, where *P* represents the observed splitting parameters (ϕ or δt), θ is the modulo of the BAZ in the first quadrant, and $n = 1,2,3$ [*Silver and Savage*, 1994]. Therefore, plotting the splitting parameters against modulo-90° BAZ is a widely used effective approach to identify the existence of two-layered anisotropy.

2. Previous Shear Wave Splitting Studies

As summarized in Figure 1, seismic anisotropy beneath the TSOB and adjacent areas has been investigated by a number of SWS studies [*Makeyeva et al*., 1992; *Vinnik et al*., 1992; *Wolfe and Vernon*, 1998; *Herquel and*

Tapponnier, 2005; *Li and Chen*, 2006; *Huang et al*., 2011]. These studies played an important role in providing constraints on various models for the formation, structure, and dynamics of the TSOB. With the exceptions of *Vinnik et al*. [2007] and *Li et al*. [2010], which investigated complex anisotropy beneath a single station (WUS) located at the northern rim of the Tarim Basin (Figure 1), all the other studies were conducted under the assumption of simple anisotropy. Consequently, the splitting parameters were reported in the form of station-averaged values. Azimuthal variations of the splitting parameters, which are indicators of complex anisotropy [*Silver and Savage*, 1994], cannot be identified or characterized using station-averaged splitting parameters.

The earliest regional-scale SWS study targeting the TSOB was conducted by *Makeyeva et al*. [1992], who used SKS data from 18 analog seismic stations and reported nearly E-W fast orientations in western and central Tian Shan except for three stations in the Issyk Kul area, where nearly N-S fast orientations were observed (Figure 1). They suggested that a mantle flow system associated with a rising mantle plume is responsible for the observed anisotropy.

Wolfe and Vernon [1998] measured station-averaged SKS splitting parameters at 12 digital stations in the Kyrgyzstan Broadband Seismic Network (KNET) and hypothesized the existence of a complex mantle flow system produced by small-scale convection. They suggested mechanical decoupling between the crust and the uppermost mantle, and proposed that mantle flow below the Tian Shan is not related to the presumed crustal shortening caused by the continuous indentation of India into the Eurasian plate.

Herquel and Tapponnier [2005] obtained teleseismic SKS and SKKS data from seven broadband stations located in the western Tibetan Plateau and the Tarim Basin (Figure 1). They conducted SWS analyses using the rotation-correlation method and obtained dominantly NE-SW fast orientations and proposed two competing mechanisms for the observed anisotropy: underthrusting of the Tarim lithosphere beneath the Tibetan Plateau and frozen-in anisotropy within the Precambrian lithosphere.

SWS analyses were carried out by *Li and Chen* [2006] using SKS data recorded by 30 stations in central Tian Shan, northern Tarim Basin, and the Kazakh Shield. The stations are predominantly from the portable GHENGIS network, which was operated for almost 3 years (October 1997 to August 2000). The resulting SWS measurements show fast orientations that are subparallel to the trend of the TSOB. Additionally, NNE-SSW fast orientations observed by *Li and Chen* [2006] in the Issyk Kul (Figure 1) and the area 200 km south of Issyk Kul were used to suggest that regional-scale convection pervaded the sublithospheric mantle beneath the Tian Shan. These NNE-SSW polarizations are approximately analogous with the surface velocity of the central Tian Shan [*Abdrakhmatov et al*., 1996] and were consequently hypothesized to be generated by basal shear due to lithosphere-asthenosphere relative motion. In addition, the study of *Li and Chen* [2006] revealed the fact that E-W splitting parameters are at high angle with the NW-SE Talasso-Fergena right-lateral strike-slip fault (Figure 1) and suggested little or no impact of the fault on the observed anisotropy.

Vinnik et al. [2007] used a data set recorded by 10 broadband stations, among which 2 are from the GHENGIS network and 8 are from permanent networks including IRIS/GSN, Geoscope, and KNET, to conduct joint analysis of P-to-S receiver functions and SKS particle motions. Their results show a relatively weak anisotropy and a lateral variation in the wave polarization at about 100 km depth in the mantle lithosphere, which is not mechanically coupled to the crust. These authors suggested a two-layered anisotropic model beneath station WUS (upper layer $\phi_U = -30°$ and lower layer $\phi_L = 45°$), and proposed that the upper layer is due to conjugate effects of present-day thrusting and relict deformational fabrics in the crust, while the lower layer is sourced from recent uniaxial shortening in the asthenosphere.

Li et al. [2010] measured SKS, SKKS, and PKS splitting parameters using data recorded by station WUS over a 20 year period. The resulting fast orientations demonstrate a systematic azimuthal variation with a 90° periodicity, suggesting the existence of two layers of anisotropy with horizontal axes of symmetry. The fast orientation of the lower layer is $\phi_L = 85° - 105°$, which is parallel to the absolute plate motion (APM) direction of the Eurasian plate in the hot spot frame [*Gripp and Gordon*, 2002]; the fast orientation of the upper layer is $\phi_U = 60° - 80°$, which is consistent with the strike of the mountain belt and is attributed to N-S lithospheric shortening [*Li et al*., 2010]. Note that the resulting two-layer parameters for WUS obtained by *Li et al*. [2010] and *Vinnik et al*. [2007] are significantly different.

A comprehensive SWS analysis beneath China including the Tian Shan was carried out by *Huang et al*. [2011] using all three XKS phases recorded by 138 seismic stations operated from 2000 to 2009 by the China

Seismic Network Data Center. Upon observing the consistency of XKS fast orientations within the Tian Shan and the regional trend of orogenic belts and active regional faults, *Huang et al*. [2011] proposed a lithospheric origin for the observed anisotropy.

Obviously, in spite of numerous studies, the existence and spatial distribution of complex anisotropy beneath the TSOB and adjacent areas, as well as the anisotropy-forming mechanisms in the area are still debated issues. In addition, the fact that only one station (WUS) was investigated for complex anisotropy, when combined with the inconsistency in the resulting two-layer parameters between the studies of *Li et al*. [2010] and *Vinnik et al*. [2007] at WUS, gives rise to the necessity of a fresh approach to these long-lived topics of interest. This work presents individual (rather than station-averaged) SWS measurements to identify and characterize complex anisotropic layering and explores its geodynamic implications.

3. Data and Methods

The teleseismic XKS data set used in this study was obtained from broadband seismic stations installed in the TSOB and adjacent areas with data archived in the IRIS (Incorporated Research Institutions for Seismology) DMC (Data Management Center). The data set was recorded by 25 stations in 6 different networks, with varying recording length spanning the period from early 1989 to early 2014.

Seismic events used were selected based on the following criteria: for PKS, the epicentral distance range is 120°–180°, and the cutoff magnitude is 5.8; for SKKS, the corresponding values are 95°–180° and 5.6; and for SKS, they are 83°–180° and 5.6 [*Liu and Gao*, 2013]. The distribution of the 693 events which provide at least one well-defined (Quality A or B, see below) measurement is depicted in Figure 2a. The majority of events were sourced from the western Pacific subduction zones and from the west coast of North and South America.

We employ the SWS procedure of *Liu and Gao* [2013], which was developed based on the minimization of transverse energy method [*Silver and Chan*, 1991] to compute SWS parameters. Seismograms are first filtered between 0.04 and 0.5 Hz and the splitting parameters are obtained by an automated procedure. An objective ranking algorithm [*Liu et al*., 2008] is applied to rank the resulting splitting parameters to qualities A (outstanding XKS arrivals on both the radial and transverse components), B (good), C (poor), and N (null, for which strong XKS energy is observed on the radial component, but is absent on the transverse component), on the basis of the signal-to-noise ratios of the original and corrected radial and transverse components. The inverse *F* test method of *Silver and Chan* [1991] is used to estimate the standard errors of the splitting parameters. Subsequently, manual checking is applied to all measurements in the data set to make necessary adjustment to the beginning and ending times of the XKS window, the filtering parameters, as well as the results of automatic ranking. As demonstrated in *Liu and Gao* [2013] and *Kong et al*. [2015] using synthetic and real XKS data, this is a very time consuming but critical step in order to obtain reliable SWS measurements.

4. Results

After manual checking, a total of 2089 pairs of well-defined XKS splitting parameters were obtained at 25 stations with a back azimuthal coverage (in the modulo-90° space) that is broad enough to make a reliable determination about the existence or absence of two-layered anisotropy. Measurements from stations with inadequate azimuthal coverages are excluded in this study, for the following reasons. As demonstrated below, a large portion of the study area possesses two-layered anisotropy and consequently, the splitting parameters are systematic functions of the back azimuth of the events [*Silver and Savage*, 1994]. For stations with two-layered anisotropy, station-averaged measurements or measurements from events in one or a few narrow azimuthal bands cannot correctly represent the true characteristics of the anisotropy structure, simply because events from different BAZ may result in different splitting parameters (e.g., *Gao and Liu* [2009] for a station on the southern Tibetan Plateau and *Yang et al*. [2014] for many stations on the North American craton). Obviously, station-averaged measurements are valuable only when it is known there is no azimuthal variation in the splitting parameters observed at the stations. However, adequate azimuthal coverage is required in order to rule out the existence of complex anisotropy and therefore, the use of a

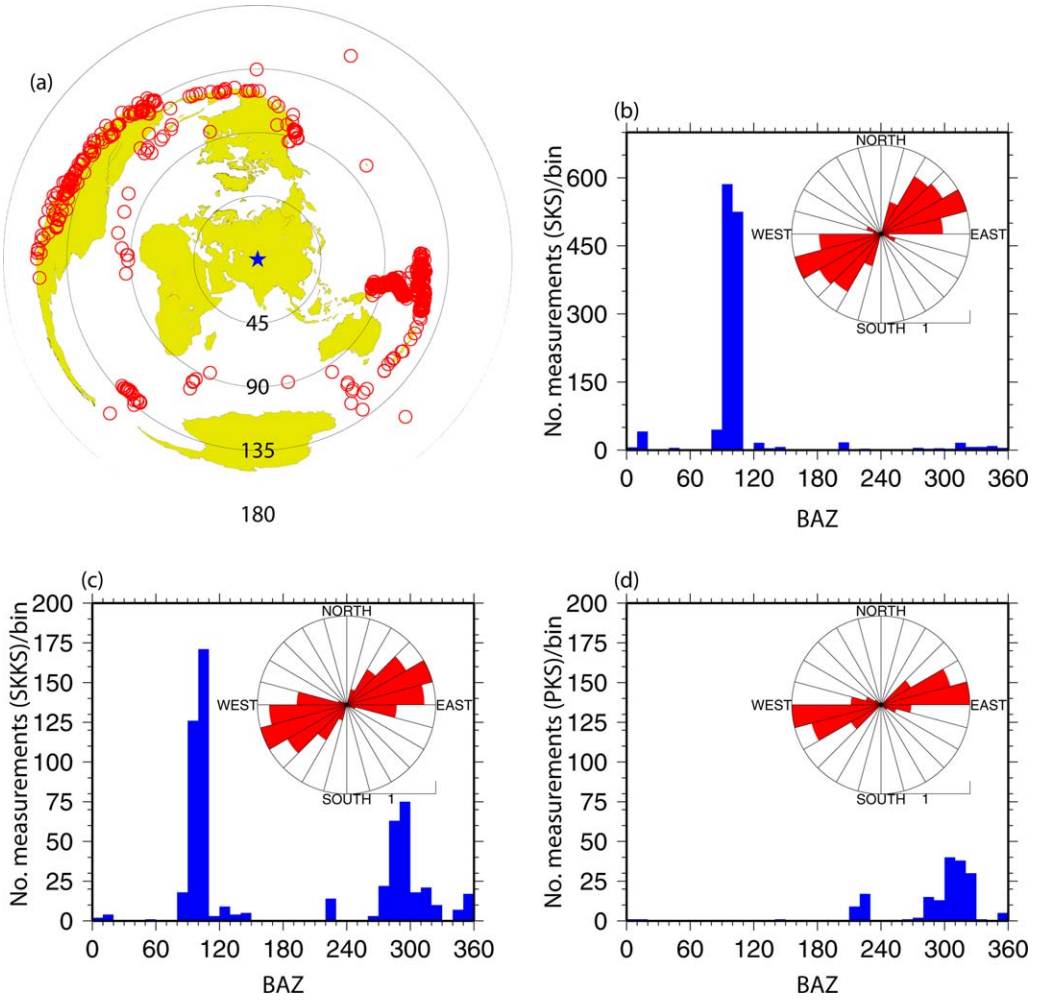

Figure 2. (a) Azimuthal equidistant projection map showing earthquakes (red circles) that contributed to at least one well-defined (Quality A or B) SWS measurement. The center of the study area is denoted by a solid star. Solid circles and corresponding labels show the distance in degrees to the center of the study area. (b) A histogram showing the back azimuth (BAZ) of the SKS measurements. The rose diagram shows resulting fast orientations using the SKS phase. (c) Same as Figure 2b but for SKKS. (d) Same as Figure 2b but for PKS.

station with inadequate BAZ coverage in an area, where the splitting parameters may truly vary with the BAZ, could lead to an undesired bias of the results.

Of the high-quality measurements from the 25 stations, 1322 are SKS, 593 are SKKS, and 174 are PKS measurements. Most of the SKS measurements have a narrow BAZ range of 90°–110° (Figure 2b), the SKKS measurements have two distinct BAZ ranges of 90°–110° and 270°–320° (Figure 2c), and PKS ones are in the BAZ range of 280°–330° (Figure 2d).

One of the most striking characteristics of the observed splitting parameters at some of the stations is a systematic azimuthal variation with a 90° periodicity, as demonstrated by the two example SKS events recorded by the same station shown in Figure 3. Such azimuthal variations can also be observed when the measurements are displayed above the ray piercing points (Figure 4). The SKS and SKKS phases produce similar results (Figures 2b and 2c), ruling out significant contributions from the lower-most mantle [*Niu and Perez*, 2004].

We visually examine the azimuthal variations of the splitting parameters observed at each of the 25 stations and find that they can be divided into two groups. Those in Group 1, which includes 10 stations, show insignificant azimuthal variations (Figures 5a–5b) in the observed splitting parameters. The majority of these stations show E-W fast orientations (Figure 6). An exception in terms of azimuthal variation is station KKAR which is located in the NW corner of the study area (Figure 4). XKS arrivals coming from the east and

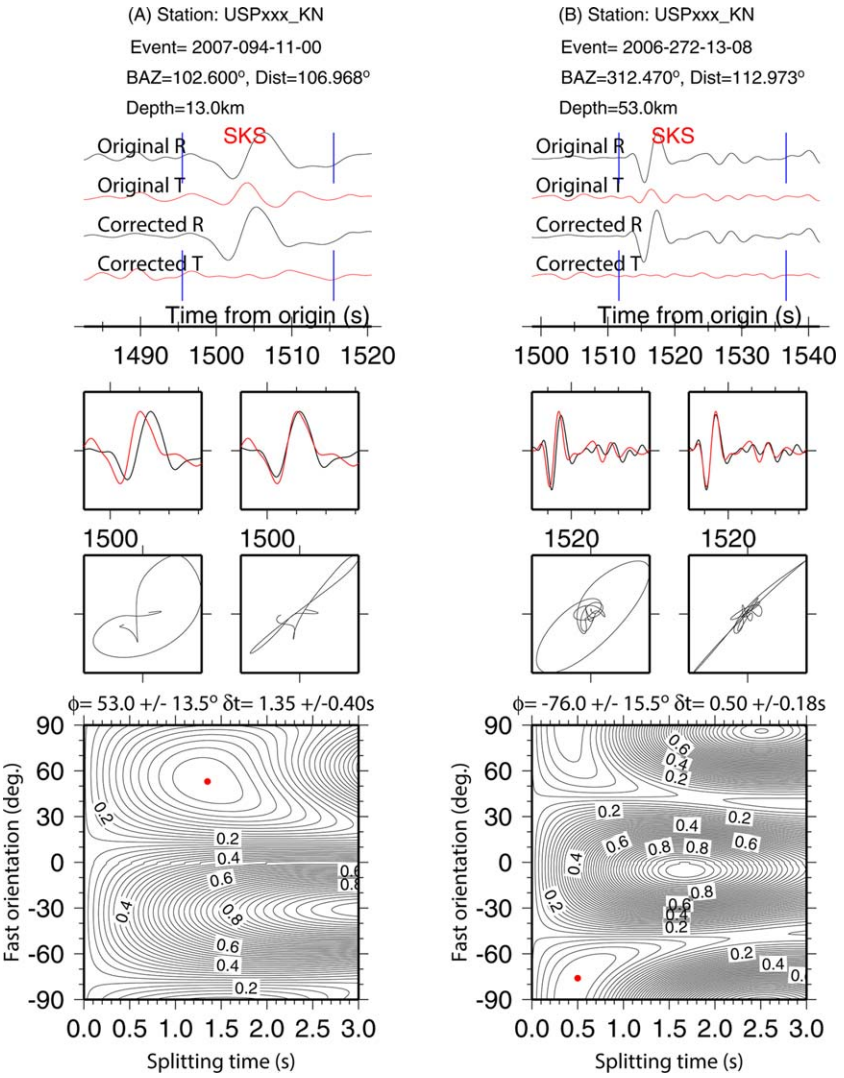

Figure 3. Examples of SWS measurements from two events recorded by one of the stations that shows back-azimuthal variations of the splitting parameters. From top to bottom, the plots show the original and corrected XKS seismograms, their particle motion patterns, and contour map of normalized energy in the corrected transverse component as a function of candidate fast orientations and splitting times. The red dot on the contour map marks the optimal splitting parameter corresponding to the minimum energy.

southeast, which sample the TSOB, show mostly NW-SE fast orientations, while those from the north and northwest, which sample the Kazakh Shield, show mostly NE-SW fast orientations. The azimuthal variation is not periodic at 90° and thus is not a consequence of multiple anisotropy layering. Instead, it might reflect spatial variations of fast orientations in the vicinity of the station. This phenomenon has been observed at a few other stations elsewhere (e.g., station ENH in central China as reported by *Liu and Gao* [2013]).

Group 2 has 15 stations, all of which are located on the northern margin of the Tarim Basin and in central Tian Shan, which is the area northeast of the Talasso-Fergana fault (Figure 1). A remarkable feature of the fast orientations observed at these stations is a clear azimuthal variation with a 90° periodicity (Figures 5c–5d and 7), indicating the existence of two-layered anisotropy.

5. Discussion

5.1. Relationship With Previous Studies

Previous studies at all but one (WUS) of the stations were performed under the assumption of simple anisotropy. Consequently, the results were presented in the form of station-averaged parameters (Figure 1), which

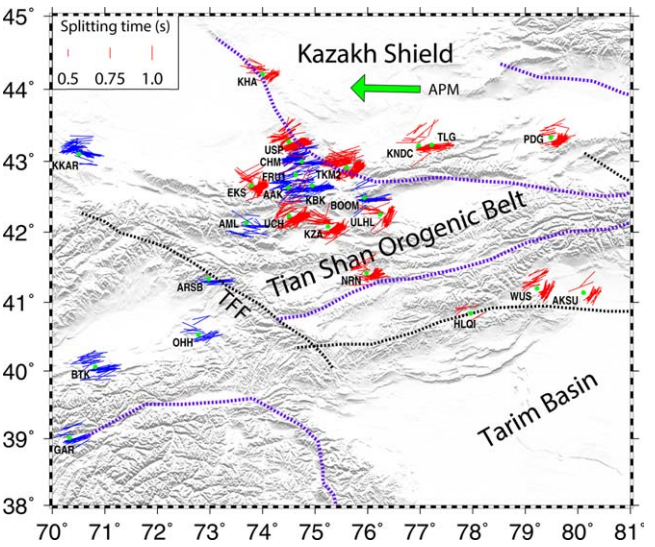

Figure 4. Resulting XKS splitting parameters for Group 1 (simple anisotropy; blue bars) and Group 2 (two-layered anisotropy; red bars) stations plotted above 100 km ray-piercing points superimposed on a digital elevation map. The green arrow indicates the absolute plate motion direction of the Eurasian plate [*Gripp and Gordon*, 2002]. The green dots represent stations.

are in good agreement with the station-averaged values observed at the stations in Group 1 by this study (Figures 6 and 8). The fast orientations at most of these stations are dominantly parallel to the strike of the TSOB and were attributed to either vertically coherent lithospheric shortening, or strike-parallel mantle flow by previous studies [*Makeyeva et al.*, 1992; *Vinnik et al.*, 2007].

A major debate in previous studies, however, was the existence, characteristics, and formation mechanisms of a zone with "anomalous" NNE-SSW fast orientations in the vicinity of the Issyk Kul (Figure 1), where most of the stations belong to Group 2 (Figure 8). A comparison of the spatial distributions of the stations used in previous studies (Figure 1) and this study (Figure 8) suggests that the majority of the stations in this area do not have adequate azimuthal coverage and thus are not used in this study. For the several stations with adequate azimuthal coverage and examined here (PDG, KZA, and NRN), the majority of the SKS events have a back azimuth of 90°–110° (or 0-20° in the modulo-90° domain; Figure 2b), and many of the measurements from events in this BAZ range show NNE-SSW fast orientations (Figure 5c). Thus, if only the SKS phase were used, the resulting fast orientations observed at the stations would be NNE-SSW, which would be consistent with previous studies that used only the SKS phase [e.g., *Li and Chen*, 2006].

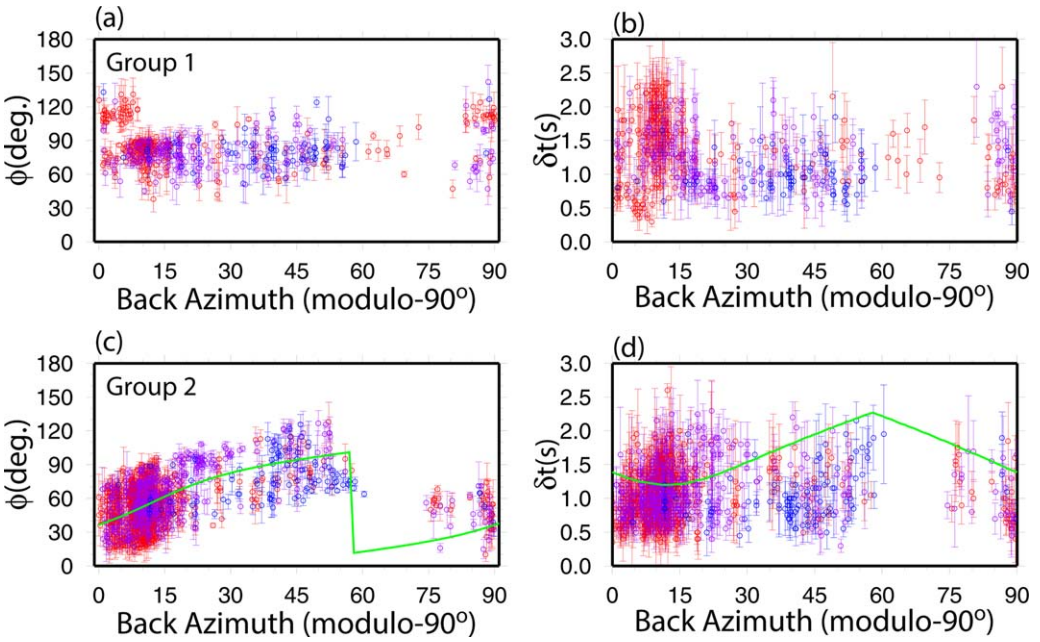

Figure 5. Azimuthal variations of all of the resulting SWS parameters plotted again modulo-90° BAZ. (a and b) are measurements from Group 1 stations, and (c and d) are those from Group 2 stations. Red, purple, and blue symbols are SKS, SKKS, and PKS measurements, respectively. The solid line in Figures 5c and 5d are theoretical apparent splitting parameters computed using a nominal period of 5 s and $\phi = -65°$ and $\delta t = 1.7$ s for the lower layer, and $\phi = 77°$ and $\delta t = 1.4$ s for the upper layer.

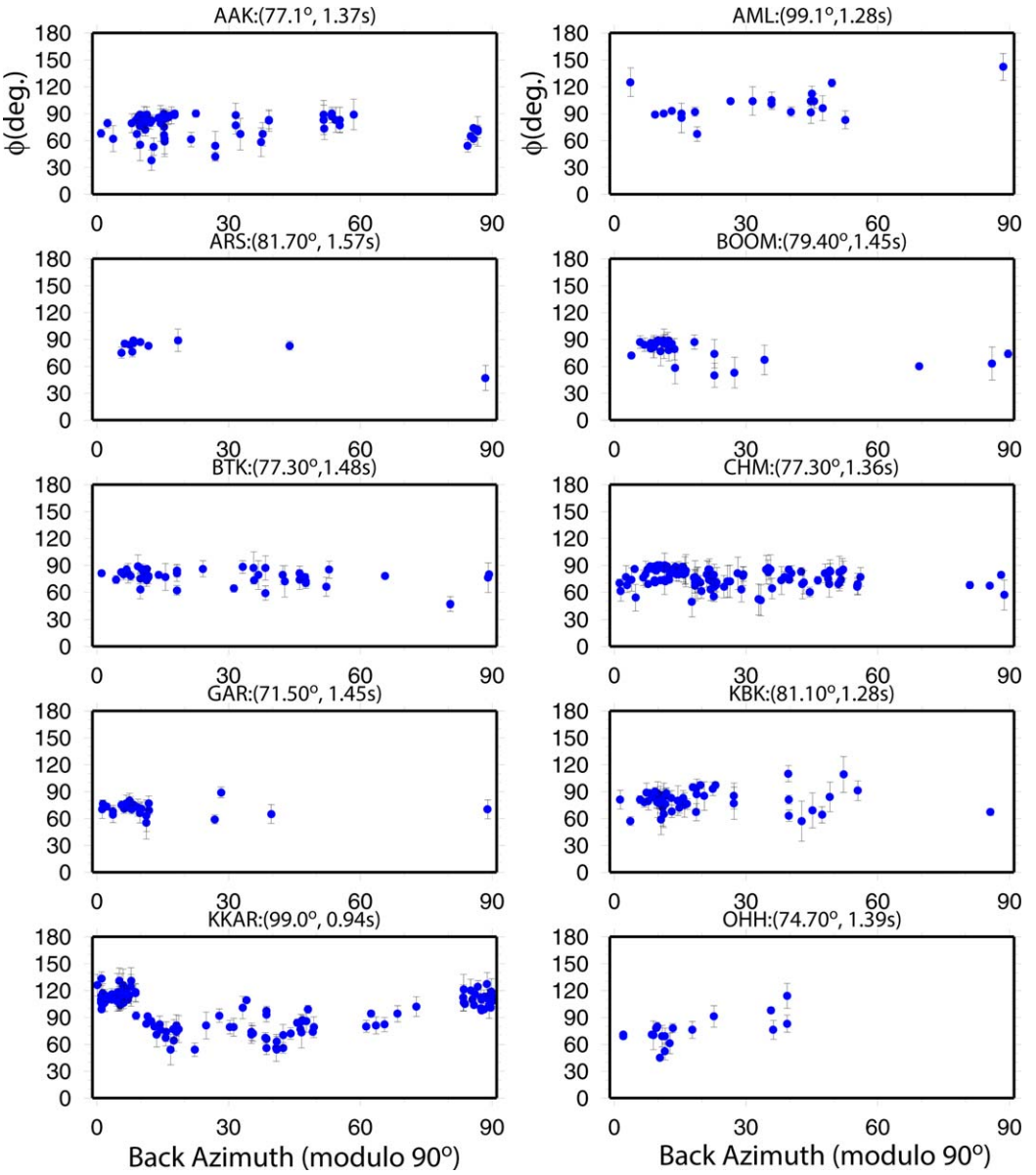

Figure 6. Azimuthal variations of observed fast orientations for each of the Group 1 stations. Values in the parentheses following the station name are station-averaged fast orientation and splitting time.

This could explain the anomalous station-averaged fast orientations in the vicinity of the Issyk Kul area (Figure 1) reported by some of the previous studies [*Makeyeva et al*., 1992; *Wolfe and Vernon*, 1998; *Li and Chen*, 2006], because most of them only used the SKS phase which has a narrow back azimuthal range. For instance, the study of *Li and Chen* [2006] used only the SKS phase and all the 17 events are in a narrow BAZ band of 98°–107°. In addition, most of the stations with anomalous fast orientations only have one or two events. The observations suggest that in areas that potentially possess complex anisotropy, events from wide back azimuthal bands, if available, should be utilized in order to reveal the true anisotropic structure.

5.2. Quantifying Two-Layer Models of Anisotropy

Previous studies conducted in the TSOB have proposed the existence of two layers of anisotropy beneath station WUS (Figure 1) and suggested various models to explain the source of anisotropy and its geodynamic implications [*Vinnik et al*., 2007; *Li et al*., 2010]. As shown in Figures 6 and 7, in addition to WUS, more than half of the 25 stations with adequate azimuthal coverage show periodic variations in the observed splitting parameters. Such variations suggest a wide spread existence of two-layered anisotropy, which, in

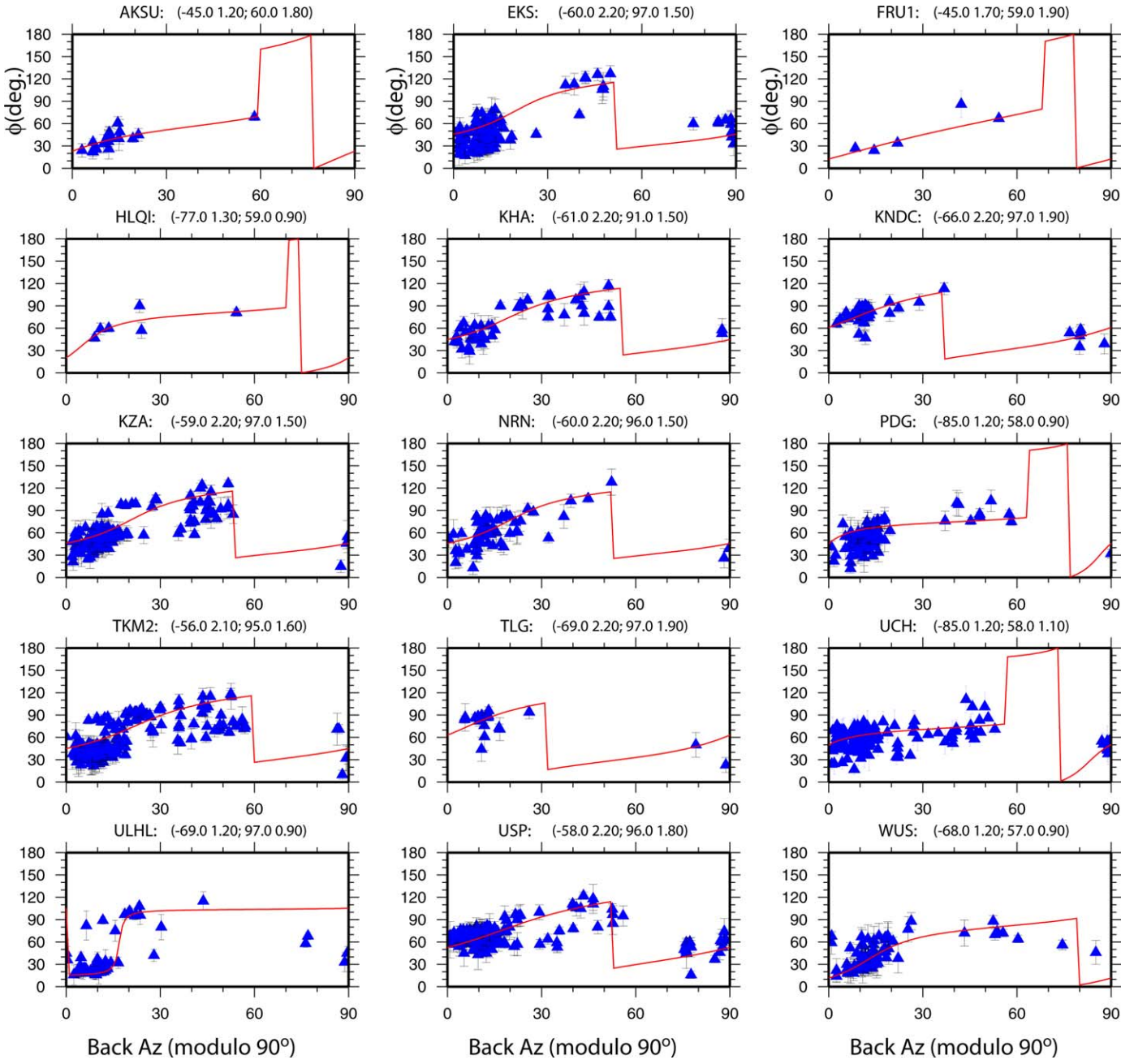

Figure 7. Same as the previous figure but for Group 2 stations. The solid curve in each of the plots shows the theoretical apparent splitting parameters computed using the optimal ϕ and δt for the lower and upper layers, which are indicated in the parentheses after the station name.

principle, can be quantified using the technique initially proposed by *Silver and Savage* [1994] by grid-searching for the two pairs of splitting parameters using measurements obtained at each of the stations.

In practice, however, measurements from individual stations are usually insufficient to produce well-constrained splitting parameters for each of the two layers. Such station-specific determinations are possible only at stations that recorded numerous high-quality XKS waveforms originated from events in a broad azimuthal range (e.g., station ATD in the Afar Depression reported by *Gao et al.* [2010], and station LSA on the Tibetan Plateau in *Gao and Liu* [2009]). For stations with limited data quality and/or quantity, reliable two-layer parameters can be obtained by combining measurements from stations with similar patterns of azimuthal variations (e.g., *Yang et al.* [2014] for the North American craton, and *Wu et al.* [2015] for the

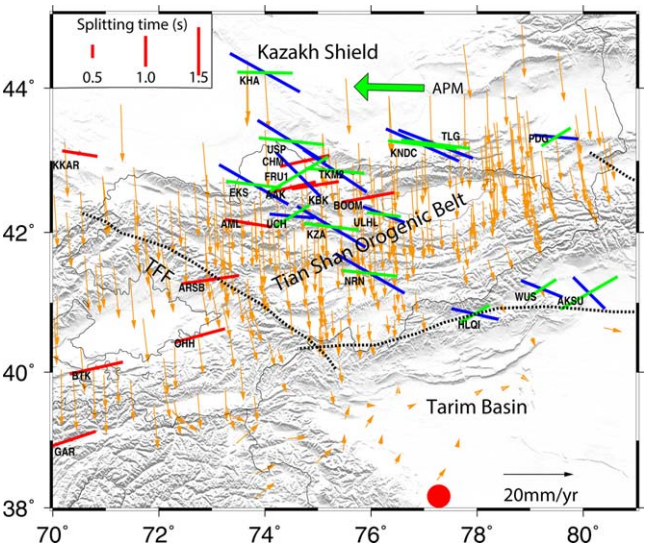

Figure 8. Station-averaged splitting parameters for Group 1 stations (red bars), and two-layer parameters for Group 2 stations (blue: lower layer; green: upper layer). Orange arrows are GPS measurements [*Zubovich et al.*, 2010] relative to the red dot in the Tarim Basin.

western Tibetan Plateau). Once the two-layer parameters are obtained using the combined data set, station-specific parameters can be estimated by using the former as constraints.

We grid-search for the two-layer parameters using all the 1557 measurements obtained at the 15 stations in Group 2. The searching range for the fast orientations is −90° to 90° with an increment of 1°, and that for the splitting times is 0–3 s with a step of 0.1 s. For each set of candidate splitting parameters, we compute the theoretical apparent splitting parameters using the relationships between the apparent splitting parameters and the two pairs of splitting parameters characterizing the two-layered model [*Silver and Savage*, 1994], and then compute a weighted misfit between the calculated and observed splitting parameters [*Gao and Liu*, 2009], i.e.,

$$\chi^2=\sum_{i=1}^{N} w_1 * [(\phi_i^{obs}-\phi_i^{cal})/\sigma_{\phi_i}]^2+w_2 * [(\delta t_i^{obs}-\delta t_i^{cal})/\sigma_{\delta t_i}]^2, \quad (1)$$

where σ_{ϕ_i} and $\sigma_{\delta t_i}$ are the standard deviation of the ith ϕ and δt measurements, respectively, N is the total number of pairs of splitting parameters, and $w_1=0.8$ and $w_2=0.2$ are the corresponding weighting factors for the ϕ and δt observations. Note that because the fast orientations show much stronger azimuthal variations than the splitting times, a larger weighting factor is assigned to the ϕ measurements. The optimal set of parameters that best represents the characteristics of the azimuthal variations of the apparent splitting parameters has a ϕ of −65° and a δt of 1.7 s for the lower layer, and a ϕ of 77° and a δt of 1.4 s for the upper layer (Figures 5c-5d). In the following, the above resulting parameters using the combined data set are called $\phi_L^{(c)}$, $\delta t_L^{(c)}$, $\phi_U^{(c)}$, and $\delta t_U^{(c)}$.

We next estimate station-specific splitting parameters by using the two-layer parameters obtained from the combined data set as constraints. Specifically, the searching range for the fast orientations of the upper and lower layers is limited to $\phi_U^{(c)}\pm20°$ and $\phi_L^{(c)}\pm20°$, respectively, and that for the splitting times is limited to $\delta t_U^{(c)}\pm0.5$ s and $\delta t_L^{(c)}\pm0.5$ s, respectively.

The resulting station-specific two-layer parameters are given in Table 1, and the theoretical apparent splitting parameters computed using the two-layer parameters for each of the 15 Group 2 stations are shown in Figure 7. At most of the stations, the fast orientation for the lower layer is WNW-ESE, while that of the upper layer is mostly parallel to the local trend of the TSOB (Figure 8). Good examples of such parallelism are found at the three stations on the northern edge of the Tarim Basin (Figure 8). Note that for some of the two-layered stations, the fast orientations between the top and bottom layers are about 15° from being parallel (e.g., TLG and ULHL) or orthogonal (e.g., AKSU and FRU1) from each other. As demonstrated by both the observed and theoretical data shown in Figure 7, these seemly small differences are sufficient to produce significant azimuthal variations with a 90° periodicity. The two-layer splitting parameters at WUS from this study are (−68°, 1.2 s) for the lower layer, and (57°, 0.9 s) for the upper layer (Figure 8). They are similar to the results of *Li et al.* [2010], but are significantly different with the findings of *Vinnik et al.* [2007] who reported an upper layer ϕ of −30° and a lower layer ϕ of 45°.

In spite of the significant difference in the spatial resolution between SWS and surface wave tomography studies, the resulting spatial distribution of the two-layer parameters is in general agreement with a recent surface wave anisotropy study [*Pandey et al.*, 2015], which shows dominantly NW-SE fast orientations in the

Table 1. Station-Averaged Splitting Parameters for Group 1 Stations and Two-Layer Parameters for Group 2 Stations

Station	Lat. (°)	Lon. (°)	No. Events	ϕ_L (°)	δt_L (s)	ϕ_U (°)	δt_U (s)
Group 1: Single-Layered Anisotropy							
AAK	42.64	74.59	71			77.1	1.37
AML	42.13	73.69	21			99.1	1.28
ARSB	41.33	72.97	12			81.7	1.57
BOOM	42.49	75.94	34			79.4	1.45
BTK	40.06	70.82	43			77.3	1.48
CHM	43.00	74.75	123			77.3	1.36
GAR	39.01	70.33	27			71.5	1.45
KBK	42.66	74.95	59			81.1	1.28
KKAR	43.10	70.51	124			99.0	0.94
OHH	40.53	72.78	18			74.7	1.39
Group 2: Two-Layered Anisotropy							
AKSU	41.14	80.11	21	−45.0	1.2	60.0	1.8
EKS	42.66	73.78	144	−60.0	2.2	97.0	1.5
FRU1	42.81	74.63	5	−45.0	1.7	59.0	1.9
HLQI	40.84	77.96	6	−77.0	1.3	59.0	0.9
KHA	44.21	74.00	48	−61.0	2.2	91.0	1.5
KNDC	43.22	76.97	54	−66.0	2.2	97.0	1.9
KZA	42.08	75.25	184	−59.0	2.2	97.0	1.5
NRN	41.42	75.98	62	−60.0	2.2	96.0	1.5
PDG	43.33	79.49	106	−85.0	1.2	58.0	0.9
TKM2	42.92	75.60	250	−56.0	2.1	95.0	1.6
TLG	43.25	77.22	20	−69.0	2.2	97.0	1.9
UCH	42.23	74.51	223	−85.0	1.2	58.0	1.1
ULHL	42.25	76.24	84	−69.0	1.2	97.0	0.9
USP	43.27	74.50	241	−58.0	2.2	96.0	1.8
WUS	41.20	79.22	109	−68.0	1.2	57.0	0.9

upper mantle for the Tian Shan area. The deeper layers (e.g., 125 and 175 km) have fast orientations that depart more from the E-W direction than the shallower layers [see *Pandey et al*., 2015, Figure 1].

5.3. Previously Proposed Anisotropy-Forming Mechanisms

E-W oriented anisotropy observed in the lower layer beneath WUS was previously attributed to APM-induced LPO in the asthenosphere [*Li et al*., 2010]. However, the NW-SE oriented anisotropy in the lower layer observed at most of our Group 2 stations makes a large angle with the westward motion of the Eurasian plate in a fixed hot spot frame (Figure 8), and thus may not be associated with APM-induced simple shear. This is consistent with the conclusion made by *Silver* [1996], who suggested that Eurasia is a slow-moving plate and thus cannot produce a significant drag shear against the underlying asthenosphere to generate significant APM-parallel anisotropy.

Liu et al. [2007] investigated the possibility of density-anomaly-driven small-scale convection beneath Tian Shan using the finite element method combined with the marker-and-cell technique. Their findings led them to hypothesize that density-driven small-scale upper mantle convection existed beneath Tian Shan as the result of an upwelling of hot and weaker upper mantle beneath the orogenic belt. The fast orientations in our study (Figure 8) do not show a north-to-south clockwise rotation of fast polarizations predicted by *Liu et al*. [2007], but rather show a generally dominant upper-layer fast orientation parallel to the strike of the orogenic belt and surface geological features, and a NW-SE oriented lower-layer anisotropy. Thus, the small-scale convection model cannot adequately explain the orientation of measurements in the study area.

It has also been suggested [*Li and Chen*, 2006] that regional-scale resistive basal shear between the relatively northward moving lithosphere and the asthenosphere would orient olivine crystals in the direction of the plate movement, and produce the NNE-SSW fast orientation observed in the Issyk Kul area (Figure 1). Surface velocity vectors obtained from GPS measurements show a prominent southward motion of the lithosphere in the TSOB with reference to the Tarim Basin (Figure 8). If the drag shear due to the relative lithosphere-asthenosphere movement is the origin of anisotropy, fast orientations throughout the TSOB would be oriented N-S consistent with the surface movement direction. In contrast, our results show that most of the fast orientations are parallel to the belt (Figure 8). Thus, the proposed model advocating basal drag does not adequately fit with our SWS measurements.

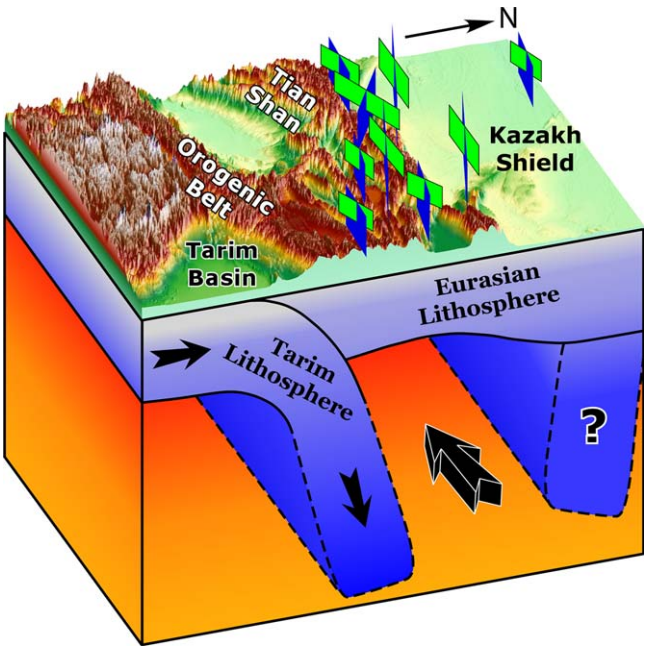

Figure 9. A cartoon showing the formation mechanisms of the observed two-layered anisotropy. The northward subduction of the Tarim lithosphere toward the thickened Eurasian lithosphere [*Lei and Zhao*, 2007], with possible southward foundering of the Kazakh slab [*Li et al*., 2009], produces WNW directed flow, which is responsible for the observed lower-layer anisotropy (blue planar bars). North-south compression and lithospheric shortening leads to E-W oriented upper-layer anisotropy (green planar bars).

5.4. Lithospheric Contributions

The station-averaged fast orientations at all Group 1 stations and the fast orientation of the upper layer at Group 2 stations are mostly E-W, which is roughly parallel to the main strike of the TSOB and orthogonal to the shortening direction revealed by GPS (Figure 8). Therefore, the simplest model is that they reflect the direction of lithospheric fabrics and olivine LPO associated with the TSOB, as suggested by *Li et al*. [2010] for the upper layer beneath WUS.

It is believed that in collisional belts, the fast orientation is analogous to the strike of structural fabrics or surface geological features suggesting coherent deformation of the lithosphere [*Silver and Chan*, 1991; *Liu et al*., 1995; *Silver et al*., 2001]. The Tian Shan is one of the most active intracontinental orogenic belts, having been shaped in response to the India-Eurasia collision [*Molnar and Tapponnier*, 1975], and is characterized by N-S crustal shortening at a rate of ~20 mm/yr [*Abdrakhmatov et al*., 1996; *Vinnik et al*., 2007; *Zubovich et al*., 2010], indicating the transfer of stress from the Himalayas through the Tarim Basin to the Tian Shan [*Neil and Houseman*, 1997].

Regional deformation gave rise to the approximate N-S direction of shortening, which is compensated by the E-W flow of sub-Tian Shan lithospheric mantle material orthogonal to the direction of maximum compression. In other words, the observed E-W fast orientations at Group 1 stations and for the upper layer at Group 2 stations are most likely the results of N-S compression, which produced strike-parallel lithospheric fabrics by aligning the olivine *a* axis preferably to the direction of extension [*Ribe and Yu*, 1991].

5.5. Anisotropy Related to Subduction of the Tarim Lithosphere

Previous GPS data analyses by numerous studies [e.g., *Abdrakhmatov et al*., 1996; *Reigber et al*., 2001; *Zubovich et al*., 2010] revealed that the Tarim Basin is moving toward Eurasia at a rate of ~20 mm/yr, implying high rates of tectonic deformation in the Tian Shan (Figure 8). The existence of relatively larger crustal thicknesses along the Tarim-Tian Shan boundary was proposed by *Vinnik et al*. [2006] to indicate an ongoing subduction of Tarim lithosphere beneath the Tian Shan. *Mattauer* [1986] also proposed that the rigid Tarim lithospheric block is likely subducting beneath the TSOB. In addition, tomographic image analyses [*Ghose et al*., 1998; *Guo et al*., 2006; *Lei and Zhao*, 2007; *Omuralieva et al*., 2009; *Lei*, 2011] suggested the subduction of the Tarim and perhaps the Kazakh lithosphere beneath the TSOB as a result of the continuous northward indentation of India onto Eurasia. These models are substantiated by GPS data that we recalculated with respect to a fixed Tarim Basin (Figure 8).

In our preferred model (Figure 9), the Tian Shan lithosphere acts as a relatively passive entity bordered by the strong Kazakh lithosphere to the north and the subducting Tarim lithosphere to the south. As a result, the asthenospheric mantle material beneath central Tian Shan is squeezed between the subducting Tarim lithosphere and the Kazakh lithospheric root. Due to the geometry of the boundary of the Tarim and Kazakh lithospheres, the asthenospheric flow can be displaced toward the WNW direction, leading to the observed WNW-ESE fast orientations in the lower anisotropic layer beneath central Tian Shan. The lack of two-layered anisotropy beneath western Tian Shan suggests that in the study area, such a flow is only limited in central

Tian Shan. The four Group 1 stations (AAK, BOOM, CHM, and KBK) in central Tian Shan (Figure 8) might reflect lateral variations in the direction and/or strength of the flow system. For instance, a single layer of anisotropy can be created if the flow aligns with the fast orientation of the upper layer, or when the strength of the horizontal component of the flow weakens significantly due to local undulations of the bottom of the lithosphere.

6. Conclusions

A number of significant conclusions regarding mantle structure and dynamics beneath the Tian Shan can be made using a total of 2089 pairs of well-defined XKS splitting parameters obtained at 25 broadband digital seismic stations situated in the Tian Shan orogenic zone and adjacent areas.

First, among the 25 stations with adequate azimuthal coverage for a reliable determination of the existence of two-layered anisotropy, 15 of them in central Tian Shan show systematic azimuthal variations with a 90° periodicity, suggesting a wide spread existence of multilayer anisotropy in the study area. Grid searching of the two pairs of splitting parameters results in an upper layer with an ENE-WSW fast orientation, and a lower layer with a WNW-ESE fast orientation. Second, the 10 remaining stations show azimuthally invariant E-W fast orientations that are subparallel to the main strike of the Tian Shan. Third, we propose that anisotropy with a strike-parallel orientation is the result of vertically coherent lithospheric deformation, while WNW-ESE oriented anisotropy observed in the lower layer beneath central Tian Shan most likely reflects asthenospheric flow driven by the subducting Tarim lithosphere toward the thick root of the Kazakh Shield. Finally, this study demonstrates the importance of using SKS, SKKS, and PKS events from a broad azimuthal range in order to realistically reveal mantle structure and dynamics in areas with wide spread two-layered anisotropy.

Acknowledgments
The data set used for this study was obtained from the IRIS Data Management Center. We thank two anonymous reviewers for their comments. The study was partially supported by the United States National Science Foundation grant EAR-0911346 to K.L. and S.G.

References

Abdrakhmatov, K. Y., et al. (1996), Relatively recent construction of the Tien Shan inferred from GPS measurements of present-day crustal deformation rates, *Nature*, *384*, 450–453, doi:10.1038/384450a0.

Allegre, C. J., et al. (1984), Structure and evolution of the Himalaya-Tibet orogenic belt, *Nature*, *307*, 17–22, doi:10.1038/307017a0.

Avouac, J. P., P. Tapponnier, M. Bai, H. You, and G. Wang (1993), Active thrusting and folding along the northern Tien Shan and late Cenozoic rotation of the Tarim relative to Dzungaria and Kazakhstan, *J. Geophys. Res.*, *98*, 6755–6804, doi:10.1029/92JB01963.

Becker, T. W., J. B. Kellogg, G. Ekstrom, and R. J. O'Connell (2003), Comparison of azimuthal seismic anisotropy from surface waves and finite strain from global mantle-circulation models, *Geophys. J. Int.*, *155*, 696–714, doi:10.1046/j.1365-246X.2003.02085.x.

Ben Ismail, W., and D. Mainprice (1998), An olivine fabric database: An overview of upper mantle fabrics and seismic anisotropy, *Tectonophysics*, *296*, 145–158.

Bokelmann, G., E. Qorbani, and I. Bianchi (2013), Seismic anisotropy and large-scale deformation of the Eastern Alps, *Earth Planet. Sci. Lett.*, *383*, 1–6, doi:10.1016/j.epsl.2013.09.019.

Fouch, M. J., and S. Rondenay (2006), Seismic anisotropy beneath stable continental interiors, *Phys. Earth Planet. Inter.*, *158*, 292–320, doi:10.1016/j.pepi.2006.03.024.

Gao, S., P. M. Davis, H. Liu, P. D. Slack, Y. A. Zorin, V. V. Mordvinova, V. M. Kozhevnikov, and R. P. Meyer (1994), Seismic anisotropy and mantle flow beneath the Baikal rift zone, *Nature*, *371*, 149–151, doi:10.1038/371149a0.

Gao, S. S., and K. H. Liu (2009), Significant seismic anisotropy beneath the southern Lhasa Terrane Tibetan Plateau, *Geochem. Geophys. Geosyst.*, *10*, Q02008, doi:10.1029/2008GC002227.

Gao, S. S., P. M. Davis, H. Liu, P. D. Slack, A. W. Rigor, Y. A. Zorin, V. V. Mordvinova, V. M. Kozhevnikov, and N. A. Logatchev (1997), SKS splitting beneath continental rift zones, *J. Geophys. Res.*, *102*, 22,781–22,797, doi:10.1029/97JB01858.

Gao, S. S., K. H. Liu, and M. G. Abdelsalam (2010), Seismic anisotropy beneath the Afar Depression and adjacent areas: Implications for mantle flow, *J. Geophys. Res.*, *115*, B12330, doi:10.1029/2009JB007141.

Ghose, S., M. W. Hamburger, and J. Virieux (1998), Three-dimensional velocity structure and earthquake locations beneath the northern Tien Shan of Kyrgyzstan, central Asia, *J. Geophys. Res.*, *103*, 2725–2748, doi:10.1029/97JB01798.

Glorie, S., J. De Grave, M. M. Buslov, F. I. Zhimulev, D. F. Stockli, V. Y. Batalev, A. Izmer, P. van den haute, F. Vanhaecke, and M. A. Elburg (2011), Tectonic history of the Kyrgyz south Tien Shan (Albashi-Inylchek) suture zone: The role of inherited structures during deformation-propagation, *Tectonics*, *30*, TC6016, doi:10.1029/2011TC002949.

Gripp, A. E., and R. G. Gordon (2002), Young tracks of hotspots and current plate velocities, *Geophys. J. Int.*, *150*, 321–361, doi:10.1046/j.1365-246X.2002.01627.x.

Guo, B., Q. Liu, J. Chen, D. Zhao, S. Li, and Y. Lai (2006), Seismic tomography of the crust and upper mantle structure underneath the Chinese Tianshan, *Chin. J. Geophys.*, *49*(6), 1543–1551, doi:10.1002/cjg2.982.

Herquel, G., and P. Tapponnier (2005), Seismic anisotropy in western Tibet, *Geophys. Res. Lett.*, *32*, L17306, doi:10.1029/2005GL023561.

Huang, Z., L. Wang, D. Zhao, N. Mi, and M. Xu (2011), Seismic anisotropy and mantle dynamics beneath China, *Earth Planet. Sci. Lett.*, *306*, 105–117, doi:10.1016/j.epsl.2011.03.038.

Karato, S. (1989), Grain growth kinetics in olivine aggregates, *Tectonophysics*, *168*, 255–273, doi:10.1016/0040-1951(89)90221-7.

Kong, F., S. S. Gao, and K. H. Liu (2015), A systematic comparison of the transverse energy minimization and splitting intensity techniques for measuring shear-wave splitting parameters, *Bull. Seismol. Soc. Am.*, *105*, 230–239, doi:10.1785/0120140108.

Lei, J. (2011), Seismic tomographic imaging of the crust and upper mantle under the central and western Tien Shan orogenic belt, *J. Geophys. Res.*, *116*, B09305, doi:10.1029/2010JB008000.
Lei, J., and D. Zhao (2007), Teleseismic P-wave tomography and the upper mantle structure of the central Tien Shan orogenic belt, *Phys. Earth Planet. Inter.*, *162*, 165–185, doi:10.1016/j.pepi.2007.04.010.
Li, A., and C. Chen (2006), Shear wave splitting beneath the central Tien Shan and tectonic implications, *Geophys. Res. Lett.*, *33*, L22303, doi:10.1029/2006GL027717.
Li, Y., Q. Wu, L. Jiang, and R. Zhang (2010), Complex seismic anisotropic structure beneath the central Tien Shan revealed by shear wave splitting analyses, *Geophys. J. Int.*, *181*, 1678–1686, doi:10.1111/j1365-246X.2010.04589.x.
Li, Z., S. Roecker, Z. Li, B. Wei, H. Wang, G. Schelochkov, and V. Bragin (2009), Tomographic image of the crust and upper mantle beneath the western Tien Shan from the MANAS broadband deployment: Possible evidence for lithospheric delamination, *Tectonophysics*, *477*, 49–57, doi:10.1016/j.tecto.2009.05.007.
Liu, H., P. M. Davis, and S. Gao (1995), SKS splitting beneath southern California, *Geophys. Res. Lett.*, *22*, 767–770, doi:10.1029/95GL00487.
Liu, J., Q.-Y. Liu, B. Guo, D. A. Yuen, and H.-Z. Song (2007), Small-scale convection in the upper mantle beneath the Chinese Tian Shan Mountains, *Phys. Earth Planet. Inter.*, *163*, 179–190, doi:10.1016/j.pepi.2007.04.019.
Liu, K. H., and S. S. Gao (2013), Making reliable shear-wave splitting measurements, *Bull. Seismol. Soc. Am.*, *103*, 2680–2693, doi:10.1785/0120120355.
Liu, K. H., S. S. Gao, Y. Gao, and J. Wu (2008), Shear wave splitting and mantle flow associated with the deflected Pacific slab beneath northeast Asia, *J. Geophys. Res.*, *113*, B01305, doi:10.1029/2007JB005178.
Liu, K. H., A. Elsheikh, A. Lemnifi, U. Purevsuren, M. Ray, H. Refayee, B. B. Yang, Y. Yu, and S. S. Gao (2014), A uniform database of teleseismic shear wave splitting measurements for the western and central United States, *Geochem. Geophys. Geosyst.*, *15*, 2075–2085, doi:10.1002/2014GC005267.
Long, M. D., and P. G. Silver (2009), Shear wave splitting and mantle anisotropy: Measurements, interpretations, and new directions, *Surv. Geophys.*, *30*, 407–461, doi:10.1007/s10712-009-9075-1.
Makeyeva, L. I., L. P. Vinnik, and S. W. Roecker (1992), Shear-wave splitting and small-scale convection in the continental upper mantle, *Nature*, *358*, 144–147, doi:10.1038/358144a0.
Mattauer, M. (1986), Intracontinental subduction, crust-mantle decollement and crustal stacking wedge in the Himalayas and other collision belts, in *Collision Tectonics, Geol. Soc. Spec. Publ.*, *19*, 37–50, doi:10.1144/GSL.SP.1986.019.01.02.
McNamara, D. E., T. J. Owens, P. G. Silver, and F. T. Wu (1994), Shear wave anisotropy beneath the Tibetan Plateau, *J. Geophys. Res.*, *99*, 13,655–13,665.
Molnar, P., and P. Tapponnier (1975), Cenozoic tectonics of Asia: Effects of a continental collision, *Science*, *189*, 419–426.
Neil, E. A., and G. A. Houseman (1997), Geodynamics of the Tarim Basin and the Tian Shan in central Asia, *Tectonics*, *16*, 571–584, doi:10.1029/97TC01413.
Nicolas, A., and N. I. Christensen (1987), Formation of anisotropy in upper mantle peridotites-a review, in *Composition, Structure and Dynamics of the Lithosphere-Asthenosphere System, Geodyn. Ser.*, vol. 16, edited by K. Fuchs and C. Froideveaux, pp. 111–123, AGU, Washington, D. C.
Niu, F., and A. M. Perez (2004), Seismic anisotropy in the lower mantle: A comparison of waveform splitting of SKS and SKKS, *Geophys. Res. Lett.*, *31*, L24612, doi:10.1029/2004GL021196.
Ohuchi, T., and T. Irifune (2013), Development of A-type olivine fabric in water-rich deep upper mantle, *Earth Planet. Sci. Lett.*, *362*, 20–30, doi:10.1016/j.epsl.2012.11.029.
Omuralieva, A., J. Nakajima, and A. Hasegawa (2009), Three-dimensional seismic velocity structure of the crust beneath the central Tien Shan, Kyrgyzstan: Implications for large- and small-scale mountain building, *Tectonophysics*, *465*, 30–44, doi:10.1016/j.tecto.2008.10.010.
Pandey, S., X. Yuan, E. Debayle, F. Tilmann, K. Priestley, and X. Li (2015), Depth-variant azimuthal anisotropy in Tibet revealed by surface wave tomography, *Geophy. Res. Lett.*, *42*, 4326–4334, doi:10.1002/2015GL063921.
Reigber, C., G. W. Michel, R. Galas, D. Angermann, J. Klotz, J. Y. Chen, A. Papschev, R. Arslanov, V. E. Tzurkov, and M. C. Ishanov (2001), New space geodetic constraints on the distribution of deformation in Central Asia, *Earth Planet. Sci. Lett.*, *191*, 157–165, doi:10.1016/S0012-821X(01)00414-9.
Ribe, N. M., and Y. Yu (1991), A theory for plastic deformation and textural evolution of olivine polycrystals, *J. Geophys. Res.*, *96*, 8325–8335, doi:10.1029/90JB02721.
Savage, M. K. (1999), Seismic anisotropy and mantle deformation: What have we learned from shear wave splitting?, *Rev. Geophys.*, *37*, 65–106, doi:10.1029/98RG02075.
Sengor, A. M. C., B. A. Natal'in, and V. S. Burtman (1993), Evolution of the Altaids tectonic collage and Paleozoic crustal growth in Eurasia, *Nature*, *364*, 299–307, doi:10.1038/364299a0.
Silver, P. G. (1996), Seismic anisotropy beneath the continents: Probing the depth of geology, *Annu. Rev. Earth Planet. Sci.*, *24*, 385–432, doi:10.1146/annurev.earth.24.1.385.
Silver, P. G., and W. W. Chan (1991), Shear wave splitting and subcontinental mantle deformation, *J. Geophys. Res.*, *96*, 16,429-16,454, doi:10.1029/91JB00899.
Silver, P. G., and M. K. Savage (1994), The interpretation of shear-wave splitting parameters in the presence of two anisotropic layers, *Geophys. J. Int.*, *119*, 949–963, doi:10.1111/j.1365-246X.1994.tb04027.x.
Silver, P. G., S. S. Gao, and K. H. Liu (2001), Mantle deformation beneath southern Africa, *Geophys. Res. Lett.*, *28*, 2493–2496, doi:10.1029/2000GL012696.
Thompson, S. C., R. J. Weldon, C. M. Rubin, K. Abdrakhmatov, P. Molnar, and G. W. Berger (2002), Late Quaternary slip rates across the central Tien Shan, Kyrgyzstan, central Asia, *J. Geophys. Res.*, *107*(B9), 2203, doi:10.1029/2001JB000596.
Vinnik, L. P., L. I. Makeyeva, A. Milev, and A. Y. Usenko (1992), Global patterns of azimuthal anisotropy and deformations in the continental mantle, *Geophys. J. Int.*, *111*, 433–447, doi:10.1111/j.1365-246X.1992.tb02102.x.
Vinnik, L. P., I. M. Aleshin, M. K. Kaban, S. G. Kiselev, G. L. Kosarev, S. I. Oreshin, and C. Reigber (2006), Crustal and mantle of the Tien Shan from data of the receiver function tomography, *Izvestiya Phys. Solid Earth*, *42*(8), 639–651.
Vinnik, L. P., I. M. Aleshin, S. G., Kiselev, G. L. Kosarev, and L. I. Makeyeva (2007), Depth localized azimuthal anisotropy from SKS and P receiver functions: The Tien Shan, *Geophys. J. Int.*, *169*, 1289–1299, doi:10.1111/j.1365-246X.2007.03394.x.
Wolfe, C. J., and F. L. Vernon (1998), Shear-wave splitting at central Tien Shan: Evidence for rapid variation of anisotropic patterns, *Geophys. Res. Lett.*, *25*, 1217–1220, doi:10.1029/98GL00838.

Wu, J., Z. Zhang, F. Kong, B. B. Yang, Y. Yu, K. H. Liu, and S. S. Gao (2015), Complex seismic anisotropy beneath western Tibet and its geodynamic implications, *Earth Planet. Sci. Lett.*, *413*, 167–175, doi:10.1016/j.epsl.2015.01.002.

Yang, B. B., S. S. Gao, K. H. Liu, A. A. Elsheikh, A. A. Lemnifi, H. A. Refayee, and Y. Yu (2014), Seismic anisotropy and mantle flow beneath the northern Great plains of North America, *J. Geophys. Res.*, *119*, 1971–1985, doi:10.1002/2013JB010561.

Yin, A. (2010), Cenozoic tectonic evolution of Asia: A preliminary synthesis, *Tectonophysics*, *488*, 293–325, doi:10.1016/j.tecto.2009.06.002.

Zhang, S., and S. Karato (1995), Lattice preferred orientation of olivine aggregates deformed in simple shear, *Nature*, *375*, 774–777, doi:10.1038/375774a0.

Zubovich, A. V., et al. (2010), GPS velocity field for the Tien Shan and surrounding regions, *Tectonics*, *29*, TC6014, doi:10.1029/2010TC002772.